Dynamic Estimation of Full Penetration Using Geometry of Adjacent Weld Pools

Y. M. Zhang

L. Li

Welding Research and Development Laboratory,
Center for Robotics and Manufacturing Systems and
Department of Mechanical Engineering,
University of Kentucky,
Lexington, Kentucky

R. Kovacevic
Southern Methodist University,
Dallas, Texas

Control of weld penetration is currently one of the most important and crucial research issues in the area of welding. The weld pool can provide accurate and instantaneous information about the weld penetration, however, the establishment and confirmation of the correlation between weld pool and weld penetration require numerous accurate measurements and suitable geometrical modeling of weld pool. A normalized model is proposed to characterize the weld pool two-dimensionally. More than 6,000 weld pools are measured from experiments using a developed real-time weld pool sensing system. A data analysis shows that the weld penetration is correlated with the weld pool which is specified by the three characteristic parameters proposed in the study. However, the correlation is nonlinear. To approximate the complicated nonlinearity, neural networks are used. Comparative modeling trails show that the weld penetration can be more accurately calculated if the adjacent weld pools are also used. This implies that the correlation between the weld penetration and weld pool is dynamic. Hence, an on-line nonlinear dynamic estimation system is developed to estimate the weld penetration.

1 Introduction

The weld pool contains abundant information about the welding process. For example, the oscillation of the weld pool can provide sufficient information to distinguish between full and partial penetration [1, 2]. Weld pool width has been used as a rough representation of the weld penetration. Due to a recent development in sensing technology [3], clear imaging of the weld pool is possible. In a previous study, a real-time image processing algorithm was developed to extract the weld pool boundary and used to control the arc welding process [4]. By improving the hardware and algorithm, the weld pool boundary can now be obtained in 80 ms. Numerous accurate measurements can therefore be provided for studying the weld pool. It is known that skilled operators can extract information about the weld penetration by viewing the weld pool. Thus, the correlation between the weld penetration and weld pool should be studied in order to advance the sensing and control of weld penetration.

Sensing and control of weld penetration are fundamental issues of concern in automated welding. The weld penetration can be classified as partial or full penetration, which are specified by the penetration depth and back-side bead width of the weld pool respectively. For a fully penetrated pool, the back-side bead width could be sensed by a back-side sensor. However, because of limitations of sensor access and motion match between the torch and sensor, it is often necessary that the sensor be attached to and move with the torch to form a so-called top-side sensor. Thus, the top-side sensing of weld penetration is a major research issue.

The difficulty in the top-side sensing of weld penetration arises from the invisibility of the weld pool depth and back-side bead width. Indirect methods must be used. Among existing methods, pool oscillation has been extensively studied. The pioneering work was conducted by Kotecki [5], Richardson [6], Hardt [7] and their co-workers. Xiao and Ouden found an abrupt change in the oscillation frequency of the pool during the transition from the partial to full penetration [1, 2]. However, it is unlikely that the oscillation frequency can provide accurate measurements of either the penetration depth or back-side bead width of the weld pool. For example, in practical welding, the desired back-side bead width could be selected from 3 mm to 5 mm. However, the oscillation frequency is not sensitive to the variation in the back-side bead width in this range (Fig. 13 in [2]). The ultrasound based weld penetration sensing [8] has been extensively investigated at the Idaho National Engineering Laboratories [9, 10]. Although significant progress has been made, practical applications are still restricted because of the contact sensor. If the problems associated with the noncontact sensor [11] are well resolved, its extended applications can be expected. Because the temperature distribution in the weld zone contains abundant information about the welding process, infrared sensing of welding processes has been explored. Chin and co-workers have acquired valuable results in this area [12–14]. The penetration depth of the weld pool has been correlated with the infrared characteristics of the infrared image. At MIT, Song and Hardt used an infrared camera to view the temperature field from the back-side [15]. The penetration depth was precisely estimated from the measured temperature distribution and then controlled [16]. In our previous work, infrared sensing of full penetration was also been studied [17].

Because of the plasma impact, the surface of an arc weld pool is depressed. Previous researchers have found that the depression of the weld pool surface is correlative to the penetration depth of the weld pool [18, 19]. When a fully penetrated weld pool is well established, the depression will be significantly increased due to the free bottom surface of the weld pool (Fig. 11 in [20]). In this case, the size of the bottom weld pool surface plays a fundamental role in balancing the forces of the plasma impact and surface tension. Also, it is known that the surface tension is directly related with the surface curvature. Thus, the surface depression and bottom size of the weld pool are closely correlated. The back-side bead width could be estimated from the depression of the weld pool. However, the sensing of the surface depression is difficult. It was found that the average sag depression of the solidified weld bead has a good linear correlation with the back-side bead width [21]. As an alternative, a structured-light vision sensor and image processing algorithm were developed to measure the sag geome-

Contributed by the Manufacturing Engineering Division for publication in the JOURNAL OF MANUFACTURING SCIENCE AND ENGINEERING. Manuscript received Aug. 1995; revised July 1996. Associate Technical Editor: E. Kannatey-Asibe, Jr.

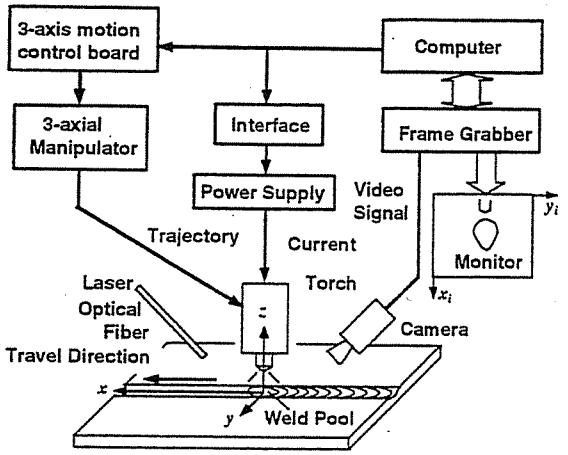

Fig. 1 Experimental set-up

try in gas tungsten arc welding. By modeling the arc welding process [22], an adaptive control system has been completed to achieve the desired back-side bead width [23]. Recently, it was found that this principle can also be used to determine the full penetration when filler wire is used. The control experimentation is currently in progress.

Although significant achievements have been made in the area of top-side penetration sensing and control, accurate and reliable techniques are still needed. Compared with the sag behind the pool rear, the weld pool could provide quicker and more accurate measurements of the welding process. If the correlation between the weld penetration and weld pool can be explored, progress will be made not only in understanding the welding process, but also in sensing and control of the welding process.

2 Experimentation

The experimental system is shown in Fig. 1. The welds are made using the DCEN gas tungsten arc welding. The welding current is controlled by the computer through its analog output to the power supply ranging from 10 A to 200 A. The torch and camera are attached to a 3-axial manipulator. The motion of the manipulator is controlled by the 3-axis motion control board which receives the commands from the computer. The motion can be preprogrammed and on-line modified by the computer in order to achieve the required torch speed and trajectory, including the arc length.

The Control Vision's ultra-high shutter speed vision system [3] is used to capture the weld pool images. This system consists of a strobe-illumination unit (pulse laser), camera head and system controller. The pulse duration of the laser is 3 ns, and the camera is synchronized with the laser pulse. Thus, the intensity of laser illumination during the pulse duration is much higher than those of the arc and hot metal. Using this vision system, better weld pool contrast can be obtained under different welding conditions than the coaxial vision system [24, 25]. The corresponding images are shown in Fig. 2(a). In our previous study, an image processing technique has been developed to extract the pool boundary. By improving the algorithm and hardware, the weld pool boundary can now be acquired on-line in 80 ms. The resultant pool boundaries are illustrated in Fig. 2(b).

The camera views the weld pool from the rear at a 45 deg angle. The frame grabber digitizes the video signals into 512 × 512 8 bit digital image matrices. The extracted boundary from the image processing is described using the image coordinate system. To obtain the actual appearance of the weld pool, the boundary should be described in the work coordinate system. The xy plane of the work coordinate system is the work surface and the z-axis is the electrode (Fig. 1). A coordinate transformation from the image coordinate to the work coordinate can be done using the camera model [26]. Thus, assume that $(x_i(j), y_i(j))$'s are the image coordinates of the weld pool boundary, the pool boundary $(x(j), y(j))$'s can be calculated from the $(x_i(j), y_i(j))$'s.

The material is stainless steel 304. The thickness of the workpiece is 3 mm. Bead-on-plate and butt welds are made. The variation in weld penetration is generated by using varied current, arc length, and travel speed (Table 1 and Fig. 3).

3 Geometrical Model of Weld Pool

The weld pool in this study refers to the two-dimensional geometry of the top-side surface view of the weld pool, and is described by the measured boundary points. However, these measured points do not directly indicate the feature of the weld pool. Also, the geometrical feature of the weld pool can not be sufficiently characterized using pool length, width, area, etc. To characterize the weld pool, a few parameters must be selected based on careful analysis. These parameters are referred to as the characteristic parameters of the weld pool.

The selection of the characteristic parameters is crucial. Three criteria must be satisfied. First, the fundamental geometrical appearance of the weld pool must be sufficiently described using the selected characteristic parameters. Secondly, the correlation between the status of the weld penetration and selected characteristic parameters must be substantial. Also, in the projected control system for weld penetration, the selected parameters must be controlled to achieve the desired weld pool and weld penetration. Although more parameters could describe the weld pool more accurately, the increase in the number of the selected characteristic parameters may complicate the resultant control system. Thus, the number of the selected parameters must not be too large. As a result, the following parametric model is proposed:

$$y_r = \pm a x_r^b (1 - x_r) (a > 0, 1 \geq b > 0) \qquad (1)$$

where a and b are the model parameters, (x_r, y_r) are the coordinates of the pool boundary in the normalized coordinate system ox_ry_r (Fig. 4). These normalized coordinates are calculated using the measured x, y coordinates:

$$\begin{cases} x_r = x/L \\ y_r = y/L \end{cases} \qquad (2)$$

where L is the length of the weld pool.

Model (1) presents a symmetric and normalized description of the weld pool. Although actual weld pools are not perfectly symmetric, if the nonsymmetry of the weld pool is not extreme, its effect on the weld penetration may be negligible. A symmetric description of the weld pool will be more suitable for correlating the weld pool to the weld penetration, in addition to reducing the number of the used parameters. In Model (1), the dimensions of the weld pool along both the length and width directions are normalized relative to the length of the weld pool. This normalized description can decouple the shape from the size of the weld pool so that the shape can be characterized by the parameters a and b. This decoupling between the shape and size can clarify the role of each parameter in characterizing the weld pool and designing a perspective control system.

The location corresponding to the maximum width of the weld pool is determined by b. It can be shown that $\max y_r(x_r) = y_r(b/(b+1))$. If the weld pool is divided into the leading and trailing portions, their lengths in the normalized coordinate system are $b/(b+1)$ and $1/(b+1)$, respectively. Thus, b is the ratio between the leading and trailing lengths. Since the trailing length is larger, $1 \geq b$. It was found that the absolute

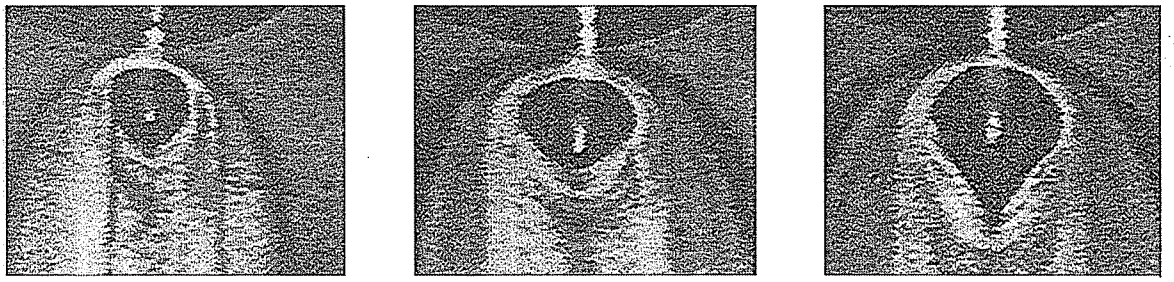

(a) Original images.

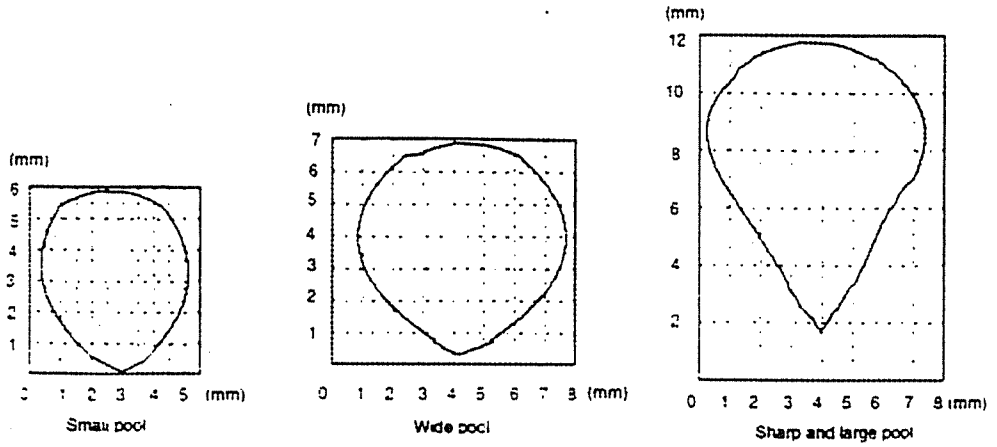

(b) Extracted pool boundaries

Fig. 2 Typical weld pools (*a*) original images (*b*) extracted pool boundaries

length of the leading portion is less seriously affected by the welding parameters than the length of the trailing portion. Thus, when the current increases, b will decrease. For a stationary weld pool, the leading and trailing lengths should be equal. In addition to b, the weld pool shape is also determined by the parameter a. For a given b, the width of the weld pool in the normalized coordinate is proportional to the parameter a. This relative width characterizes the narrowness of the weld pool and can be calculated using the parameters a and b:

$$w_r = w/L = 2a\left[\frac{b}{1+b}\right]^b \frac{1}{1+b} \tag{3}$$

Thus, the weld pool can be characterized using three parameters: the length ratio b, the relative width w_r, and the length of the pool L. These three parameters characterize the weld pool from different points of view. It is apparent that the length L is independent of the shape parameters. The shape of the weld pool is described using two independent parameters based on the narrowness and the leading to trailing ratio. Thus, these three parameters can be selected as the characteristic parameters of the weld pool and are denoted as $p_1 = L$, $p_2 = w_r$, and $p_3 = b$.

Figure 5 shows two families of simulated weld pool boundaries. In family A (Fig. 5(a)), the relative widths are the same, whereas the leading to trailing length ratios vary. It can be seen that the narrowness of the weld pools looks similar despite the variation in the ratio. In family B, the weld pools possess the

Table 1 Experimental conditions

No.	current (A)	arc-length (mm)	speed (mm/s)	gap	Ar flow rate (SCFH)
1	100	see Fig.3(a)	2	-	30
2	100	see Fig.3(b)	2	-	30
3	see Fig.3(c)	3	2	-	30
4	100	3	2	-	25
5	100	3	3	-	30
6	100	3	2.5	-	30
7	100	3	1.5	-	30
8	100	3	2	see Fig.3(d)	35

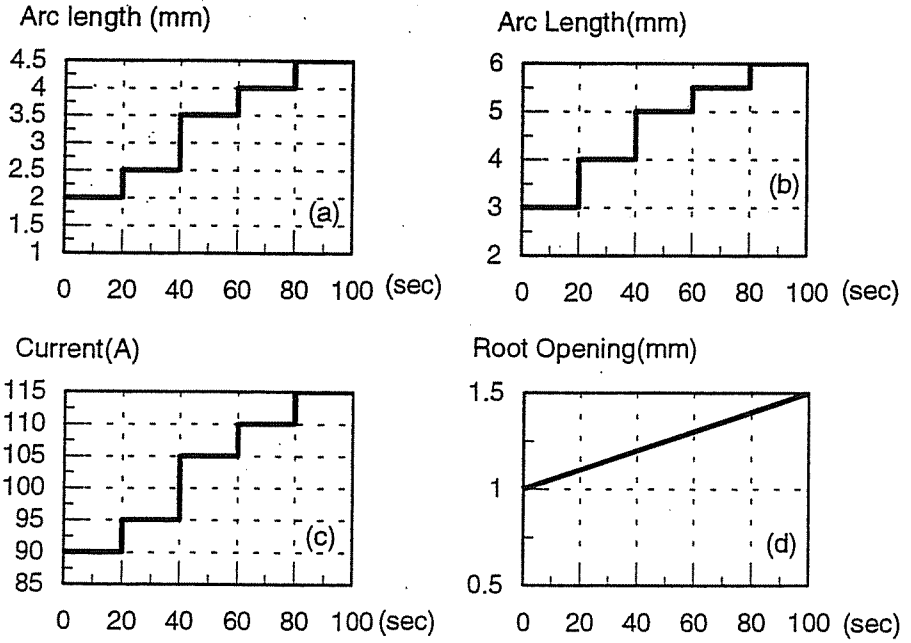

Fig. 3 Partial experimental parameters (*a*) arc length variation in experiment 1 (*b*) arc length variation in experiment 2 (*c*) current variation in experiment 3 (*d*) root opening in experiment 8

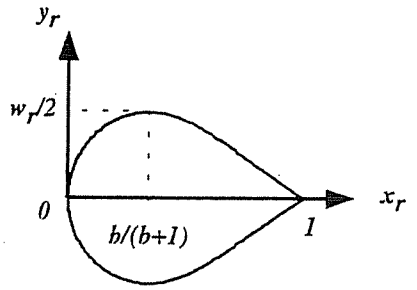

Fig. 4 Normalized Coordinate system

same leading to trailing length ratio (Fig. 5(*b*)). It can be seen that the variation in the relative width changes the narrowness of the weld pool.

The sufficiency of the selected parameters in characterizing the geometrical appearance of the weld pool can be examined by comparing practical weld pools with their modeling results. The modeling results for the weld pools in Fig. 2 are shown in Fig. 6. It can be seen that the acquired models do characterize the geometry of these typical pools. The effectiveness in characterizing the weld penetration will be discussed later.

It can be seen that the proposed model is nonlinear about the parameter b. However, its linear version can be acquired using a log transformation. Hence, the normalized parameters a and b can be on-line identified from the weld pool boundary using the linear least squares algorithm [27].

4 Nonlinear Estimation

The weld pool develops in a three-dimensional world. A top-side sensing technology needs to estimate the invisible weld penetration status from the top-side visible information. In this study, the top-side visible information is the observed weld pool and therefore two-dimensional. It is difficult to prove theoretically that the status of the weld penetration is unique for a certain top-side appearance of the weld pool. However, it is known that different variables of the welding process are heavily coupled. When a welding parameter changes, all the process variables will change accordingly. The signature of the change in a specific process variable may be detected from the changes in other process variables. The problem is how to select the coupled variables and how to correlate them.

The weld pool could contain the signature of the change in the weld penetration. In fact, for the gas tungsten arc welding process addressed in this study, the majority of the heat is input from the surface and then transferred into the metal. The heat

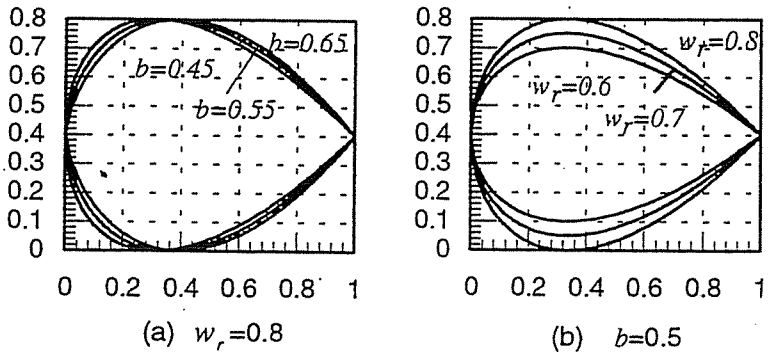

Fig. 5 Simulated weld pools (*a*) Family A (*b*) Family B

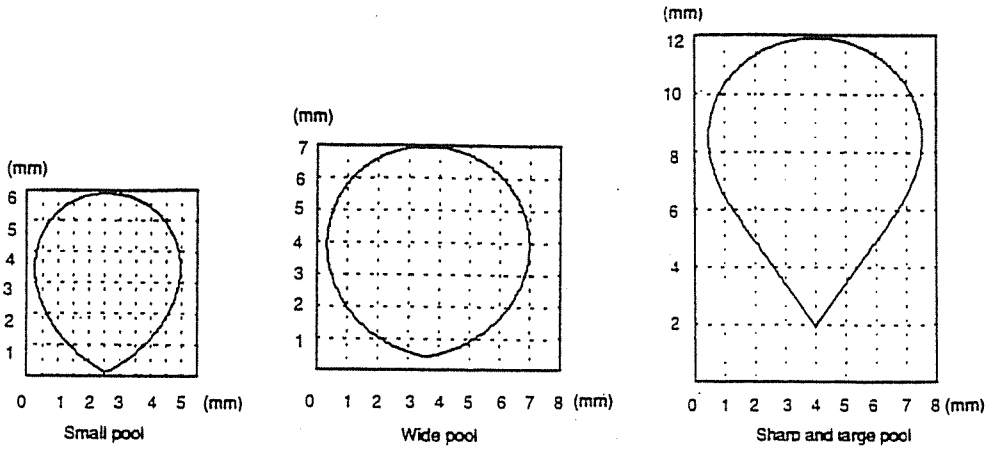

Fig. 6 Modeling results of the typical weld pools using normalized model

transfer occurring inside the metal is therefore closely correlated with the surface of the weld pool. Hence, the change in the weld penetration should leave some signature on the weld pool surface. Although the correlation between the weld pool surface and weld penetration could also be influenced by the material, welding process, and thickness, these parameters are usually known. Other welding parameters or conditions, i.e., current, travel speed, heat transfer condition, shielding gas, and angle of the electrode tip may vary during welding. However, analysis shows that the influence of these parameters on the addressed correlation may be negligible. The weld penetration could therefore be estimated using the top-side visible weld pool.

To confirm the existence of the correlation between the weld pool and weld penetration, experiments have been done using varied welding parameters (see the experimental section). The material, thickness, and welding process were not changed. The on-line image algorithm [4] was used to detect the weld pool boundary, and the characteristic parameters of the weld pool were measured at 10 Hz. Hence, numerous accurate data were acquired from different weld pools (Fig. 7). The back-side bead width was off-line measured using the structured-light technique developed in a previous study [28]. It can be seen that both the characteristic parameters and back-side bead width vary in a large range. If the variation in the back-side bead width can be tracked by using the characteristic parameters, the existence of the correlation between weld pool and weld penetration is confirmed. The remaining task will be to improve the modeling accuracy.

The cross-correlation functions between the back-side bead width and each individual characteristic parameter shows that the back-side width has significant correlation with the characteristic parameters. In order to accurately estimate the back-side bead width using the characteristic parameters, a mathematical model should be acquired. Denote the measured data as:

$$\begin{aligned} &w_b(1),\ p_1(1),\ p_2(1),\ p_3(1)\\ &w_b(2),\ p_1(2),\ p_2(2),\ p_3(2)\\ &\cdots\cdots\\ &w_b(N),\ p_1(N),\ p_2(N),\ p_3(N) \end{aligned} \tag{4}$$

where $w_b(j)$, $p_1(j)$, $p_2(j)$, and $p_3(j)$ are the back-side bead width, pool length, relative width, and length ratio at the jth sample instant, respectively. The number of samples is N, succeedingly counting from the first to the last experiment. In general, the mathematical model can be written as:

$$w_b(j) = f(p_1(j), p_2(j), p_3(j)) \tag{5}$$

The form of the functional relation f could be complicated. Its simplest form can be expressed by the following linear equation:

$$w_b(j) = \alpha_0 + \alpha_1 p_1(j) + \alpha_2 p_2(j) + \alpha_3 p_3(j) \tag{6}$$

Using the standard least square algorithm [27], this linear model can be fit from the raw data. The results are shown in Fig. 8(a). It can be seen that the measured back-side bead width can be traced with acceptable accuracy by the characteristic parameters of the weld pool. This implies that the selected characteristic parameters do contain sufficient information about the weld penetration. However, when 15 parameters from five adjacent weld pools are used to develop a linear model, no accuracy improvement is observed (Fig. 8(b)). In order to further improve the modeling accuracy, a more complicated non-linear model should be tried.

A major difficulty in non-linear modeling is the acquisition of the model structure. In our case, it is very difficult to acquire the model based on theoretical analysis. However, the artificial neural-networks can be used to approximate almost any kind of nonlinear functions if the used neurons are sufficient [29]. In our case, numerous data have been measured so that the allowed number of neurons can be large. High modeling accuracy can therefore be expected on the resultant neural network. Thus, the neural networks have been used to correlate the back-side bead width with the characteristic parameters of the weld pool in this study.

Figure 9 illustrates the neural network modeling results. One hidden layer was used in the network work. The number of neurons in the input layer equals to and varies with the number of the used inputs. The number of neurons in hidden layer should be selected so that the total number of intersections between neurons in adjacent layers is not larger than one fifth of the number of samples [30]. In our case, numerous data are available and the allowed number of neurons in the hidden layer can be very large. Although more neurons could improve the approximation capability of the network, the difficulty in the training convergence could be increased. Thus, the number of neurons in the hidden layer was selected to be 25 for all the neural networks in this study. The sigmodial function [29] was selected as the non-linear function of the neuron. The training was performed using the commercial neural network software, Professional II [30]. The algorithm is the extended delta-bar-delta (EDD) which can overcome the slow convergence associated with the conventional back-propagation algorithm [29]. The learning ratio is automatically determined by the algorithm. The training cycle is selected to be 50,000. It can be seen from Fig. 9 that the modeling accuracy associated with each individual parameter is much lower than the accuracy provided by the three characteristic parameters. A significant difference is also observed when using any two of the characteristic parameters rather than all three parameters. Thus, in order to suffi-

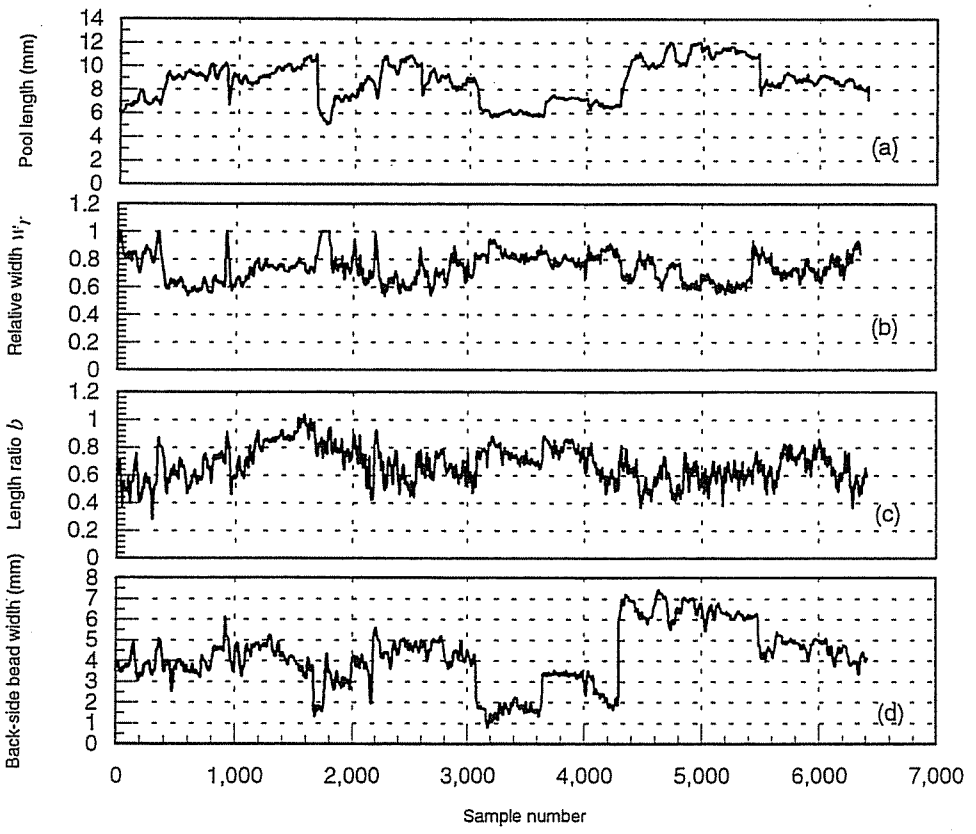

Fig. 7 Measured weld pool parameters. Data ranges for different experiments: experiment 1 from 1 to 950, experiment 2 from 951 to 1650, experiment 3 from 1651 to 2530, experiment 4 from 2531 to 3050, experiment 5 from 3050 to 3610, experiment 6 from 3611 to 4300, experiment 7 from 4301 to 5500, experiment 8 from 5501 to 6400. (*a*) pool length (*b*) relative width w_r (*c*) length ratio *b* (*d*) back-side bead width.

ciently determine the weld penetration, three characteristic parameters are used.

A comparison can be made between the linear (Fig. $8(a)$) and non-linear (Fig. $9(c)$) models. In Fig. $8(a)$, severe modeling errors are primarily observed in data ranging from 500 to 800, from 1,200 to 1,600, from 2,300 to 2,500, and from 3,500 to 4,100. It can be seen that these severe errors have been substantially reduced in Fig. $9(c)$. Thus, the nonlinearity does improve the capability of the model in approximating the studied correlation.

In order to examine the sufficiency of the selected three parameters in characterizing the weld pool from the viewpoint of determining the weld penetration, a network has also been trained to calculate the back-side bead width using a full set of weld pool parameters, including the pool length and nine widths of the weld pools equally sampled longitudinally. The modeling results are illustrated in Fig. 10. By comparing with Fig. $9(c)$, it can be found that the difference between modeling accuracies associated with the full set of parameters and the selected three characteristic parameters is very small. This implies that the

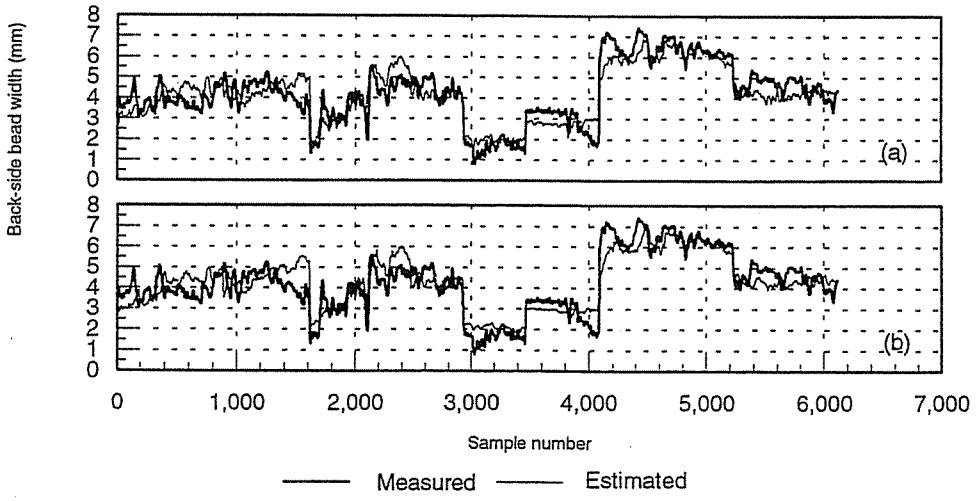

Fig. 8 Linear modeling of weld penetration using characteristic parameters of the weld pool (*a*) modeling based on the current weld pool (*b*) modeling based on adjacent weld pools

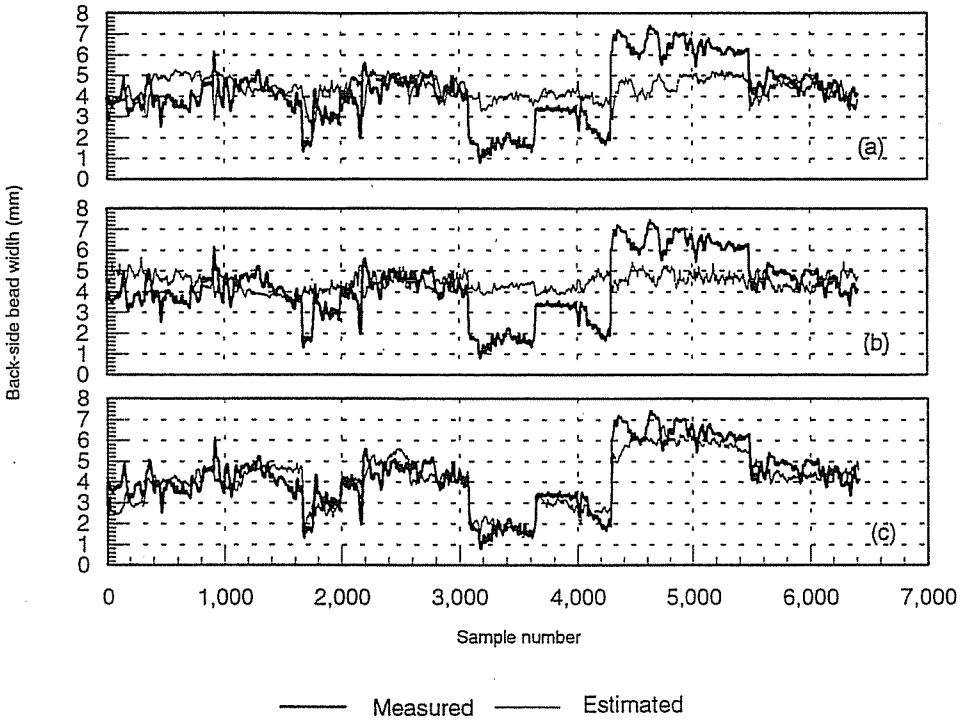

Fig. 9 Neural network based nonlinear modeling of weld penetration using different characteristic parameters of the weld pool (*a*) using the relative width (*b*) using the length ratio (*c*) using all of the three characteristic parameters

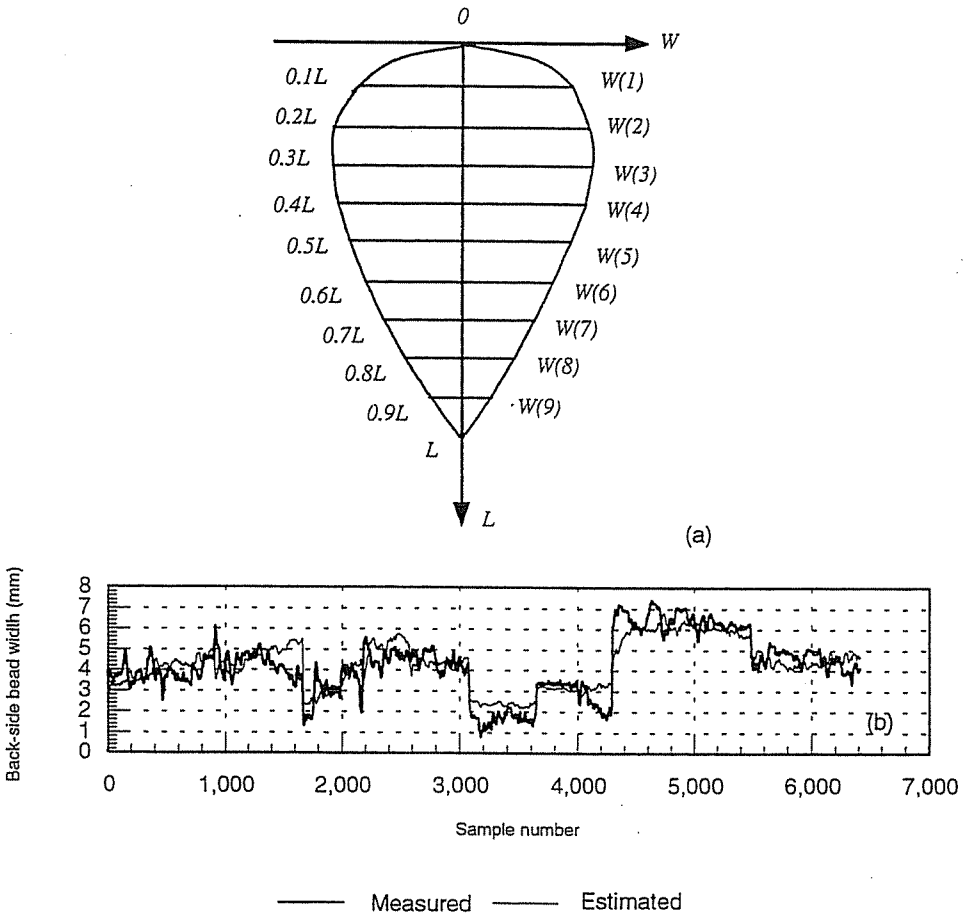

Fig. 10 Neural network modeling of weld penetration using a full description of the weld pool (*a*) definition of the full description (*b*) modeling results using L and $w(1), \ldots, w(9)$

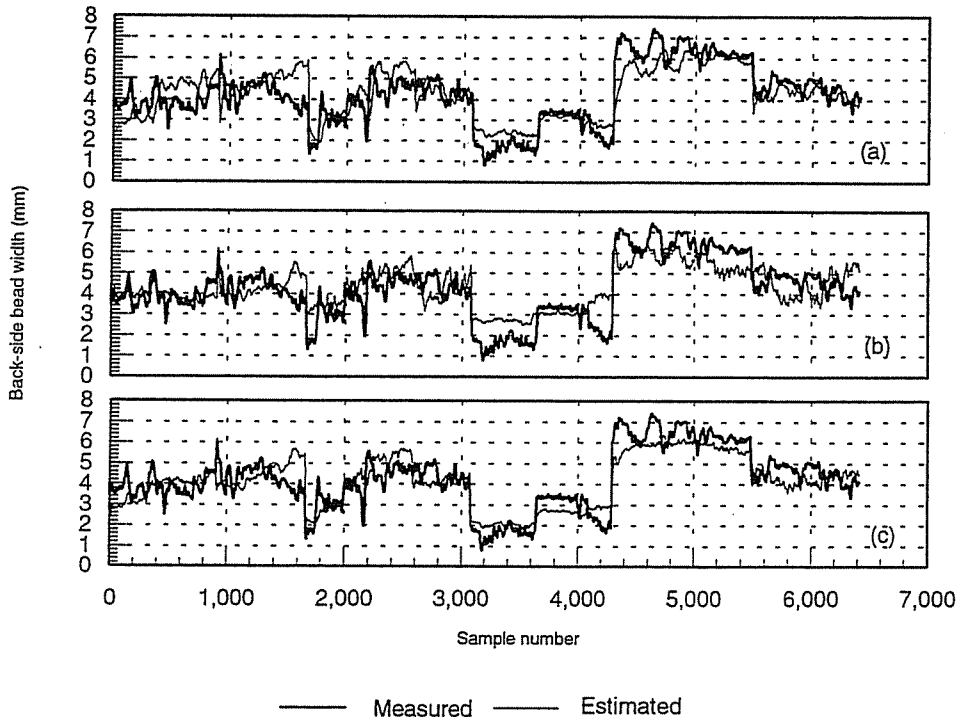

Fig. 11 Neural-network modeling of weld penetration using conventional weld pool parameters (*a*) using pool length (*b*) using pool width (*c*) using length and width

selected parameters can sufficiently characterize the weld pool for determining the weld penetration.

To show the effect of the selected characteristic parameters in acquiring the accurate estimation of weld penetration, the conventional parameters of the weld pool have also been used as the inputs for the neural networks. The results are shown in Fig. 11. It can be seen in the sample number ranging from 1000 to 1600, from 2200 to 2800, and from 3600 to 4300 that the conventional parameters do not provide the estimates of the weld penetration as accurately as the characteristic parameters do. In addition, it is apparent that the conventional parameters characterize the geometrical features of the weld pool from different points of view or independently, whereas the proposed characteristic parameters mutually characterize the weld pool. Because of more reasonable characterization, the weld penetration can be better estimated.

5 Dynamic Modeling and On-Line Estimation

The above networks are basically different realizations of the function (5) which correlates the back-side bead width to the characteristic parameters at the same instant (jth). Although the functional relationship could be sufficiently sophisticated to approximate any possible correlation between the output and inputs, the input information may not be sufficient. That is, the status of the weld penetration at any instant may not be determined only by the weld pool at the same instant, but also by the adjacent weld pools. This implies that the correlation between the weld penetration and the weld pool is dynamic. The following function should be used to correlate the weld penetration to the weld pool:

$$w_b(j) = g(\mathbf{p}^T(j + \Delta), \mathbf{p}^T(j + \Delta - 1), \ldots, \mathbf{p}^T(j + \Delta - n)) \quad (7)$$

where $\mathbf{p}^T = (p_1, p_2, p_3)$ is the characteristic parameter vector, n is the order of the dynamic model which defines the range in which the weld pool can substantially affect $w_b(j)$, and $vT\Delta$ is the shift from the current location ($x = vjT$) to the most forward location ($x = vT(j + \Delta)$) where the arc can still influence the back-side bead width $w_b(j)$ (Fig. 12). Here v and T are the torch speed and sampling period, respectively.

In our case, the characteristic parameters of the weld pool are the outputs of the welding process. The correlation between the welding input parameters (current, etc.) and resultant weld pools is dynamic due to the substantial inertia of the welding process. Thus, each individual characteristic parameter of the weld pool must be substantially auto-correlated despite the form of the welding input parameters. In the modeling of weld penetration, the characteristic parameters are the inputs. The auto-correlation in each individual input makes it difficult to estimate Δ and n based on the functions of the cross-correlation between the back-side bead width and each individual characteristic parameter. Thus, these model parameters will be determined in the modeling simultaneously with other model coefficients. Again, the neural networks are used to approximate the nonlinear function g of Eq. (7).

In general, the parameter vector $\mathbf{p}$ which can maximally affect $w_b(j)$ may be $\mathbf{p}(j + j_0^*)$, rather than $\mathbf{p}(j)$. Here j_0^* is referred to as the transfer shift. Before the dynamic modeling is performed, the transfer shift should be determined. That is, the model

$$w_b(j) = f(l(j + j_0), w_r(j + j_0), b(j + j_0)) \quad (8)$$

should be optimized with respect to the possible j_0. Thus, the optimal j_0, denoted as j_0^*, which can minimize the modeling error

$$\sum_j (w_b(j) - f(l(j + j_0^*), w_r(j + j_0^*), b(j + j_0^*))^2 = \min_{j_0} \sum_j (w_b(j) - f(l(j + j_0), w_r(j + j_0), b(j + j_0))^2 \quad (9)$$

can be acquired. It has been clearly observed that the modeling accuracy associated with $j_0 = j_0^*$ has been significantly im-

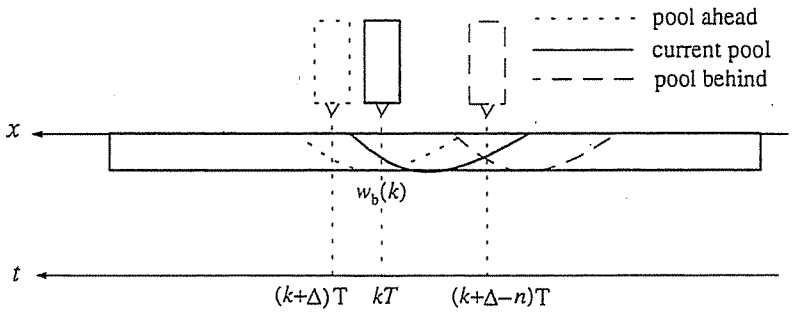

Fig. 12 Arc effect shift

proved compared with $j_0 = 0$. Also, the value of j_0^* varies from experiment to experiment because of the variations in the used welding speed and other welding parameters. However, $j_0^* > 0$ is always observed. This implies that the arc location at which the back-side bead width $w_b(j)$ will be maximally affected by the weld pool is ahead of the current electrode location $x = jTv$.

Based on the selected j_0^*, Eq. (7) can be written as

$$w_b(j) = g(\mathbf{p}^T(j + j_0^* + \delta), \mathbf{p}^T(j + j_0^* + \delta - 1), \ldots, \mathbf{p}^T(j + j_0^* + \delta - n)) \quad (10)$$

where $\delta = \Delta - j_0^*$. In this case, the number of the network inputs is $3(n + 1)$. Because of the small sampling period ($T = 0.1$ s), n could be large. The resultant input number could reach nearly one hundred. To reduce the input number, the means of the characteristic parameters were calculated for every 5 sampling period and used as inputs for the dynamic networks. Thus, the input number was significantly reduced. By extensive neural network modeling trails, the best δ and n which can minimize the modeling errors were found for each individual experiment. Although the acquired optimal δ and n are not exactly the same for different experiments, the variations in these parameters are small. The best δ varies around 5, and the best n is about 25. The neural network modeling results for different experiments are plotted in Fig. 13(a) and (b) for the static model (using both zero j_0 and zero n) and dynamic model (using non-zero j_0 and n), respectively. It can be seen that compared with Fig. 13(a), the modeling accuracy in Fig. 13(b) has been significantly improved. Thus, the correlation between the weld pool and weld penetration is substantially dynamic. Using $\delta = 5$ and $n = 25$ and all the experimental data, a dynamic neural network can also be trained using the means of the characteristic parameters for each 5 sampling period as the inputs. The modeling accuracy can be observed in Fig. 14. It is seen that despite the large variation and steep change, the back-side bead width has been well tracked by the adjacent weld pools (characteristic parameters). Significant improvement in the modeling accuracy can be observed by comparing the dynamic modeling (Fig. 14) with the static ones (Fig. 9(c)).

Using the developed image processing algorithm and dynamic neural network, a system has been developed to online estimate the back-side bead width (Fig. 15). The executive code of the trained network is directly loaded down into the personal computer 486DX100 and called by the C-program as a subroutine. The implementation of this subroutine needs only less than 13 ms. The whole cycle, including the image acquisition, image processing, geometrical modeling of weld pool boundary, and network computation, can be completed in 100 ms. In the example illustrated in Fig. 15, the welding conditions are the same as in the welding experiments. The used welding parameters are shown in the figure. The off-line measured back-side width is also shown in order to compare with the estimated results. It can be seen that the variation in the back-side bead width has been tracked with sufficient accuracy.

6 Discussion

6.1 Roles of Weld Pool Parameters. The estimated linear model is

$$w_b = -6.26 + 0.908l + 5.06w_r - 1.69b \quad (11)$$

The units for the back-side bead width and pool length are millimeters. It has been shown that this simple linear model can be used to calculate the back-side bead width of a fully penetrated weld pool with acceptable accuracy. Also, it explicitly expresses the correlation between the weld penetration status and each individual characteristic parameter. It can be seen that the back-side bead width will increase by about 0.9 mm when the pool length increases by 1 mm if the pool length is in a proper range, i.e., 5 mm to 12 mm as used in the modeling (Fig. 7(a)). For a given pool length, the weld penetration increases with increasing relative pool width. This implies that the area of the weld pool is also a factor in determining the weld penetration. A larger weld pool tends to increase the weld penetration. However, its influence on the weld penetration is not as significant as the pool length is. In fact, the range of interest of the relative width is from 0.6 to 0.9 for a moving GTA weld pool (Fig. 7(b)). Thus, the maximum change caused by the relative width is about 1.5 mm. It has been stated that the leading to trailing length ratio is an important parameter for characterizing the shape of the weld pool. In general, when the heat transfer condition becomes poorer or the current increases, the weld pool could become longer and sharper whereas the leading portion of the weld pool changes slightly. The length ratio decreases. Thus, a decrease in the length ratio should increase the weld penetration. This correlation can be seen from the negative coefficient in Eq. (11). The range of the length ratio in the raw data is from 0.4 to nearly 1, and the maximum possible change caused by the length ratio is about 1 mm. It is clear that the length plays the most important role in determining the weld penetration. However, the roles of the relative width and length ratio are also significant.

The above analysis is made based on the linear model. In order to further analyze the correlation between the weld penetration and weld pool parameters, a more sophisticated non-linear dynamic model should be used. Because the correlation given by the neural network is not explicit, the responses of the back-side bead width to the step change of each individual characteristic parameter have been calculated (Fig. 16). It can be seen that when the pool parameters change, the back-side bead width undergoes a transient period and then reaches the steady-state value. This transient period is caused by the dynamic correlation between the weld pool surface and back-side bead width. Also, it can be seen that the gains of the back-side bead width in response to the changing pool parameters vary with the weld pool parameters. (That is, the correlation is nonlinear.) However, the degrees of the nonlinearity are different. The relative width has a good

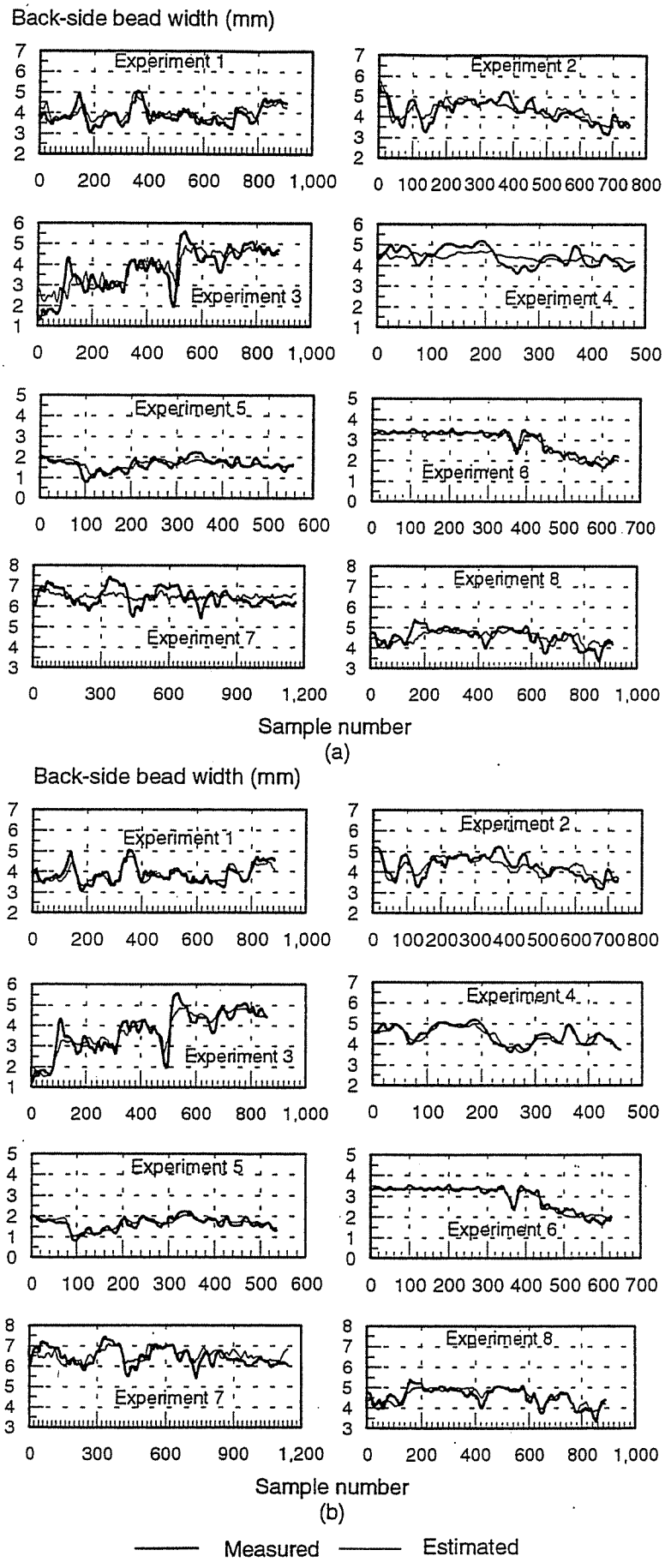

Fig. 13 Modeling for different experiments (*a*) using unshifted data (*b*) dynamic modeling

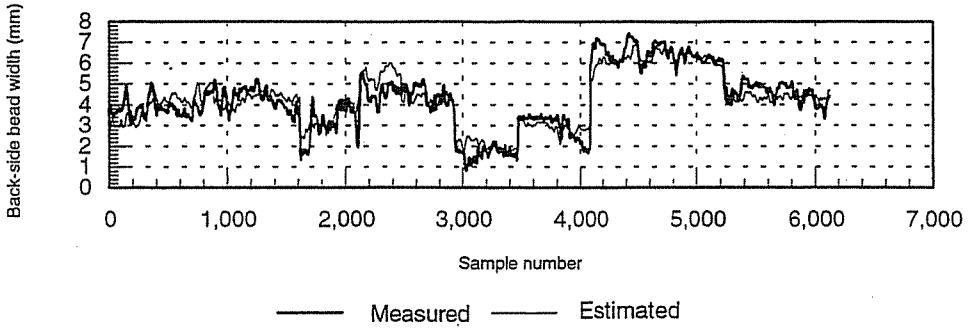

Fig. 14 Dynamic modeling of weld penetration

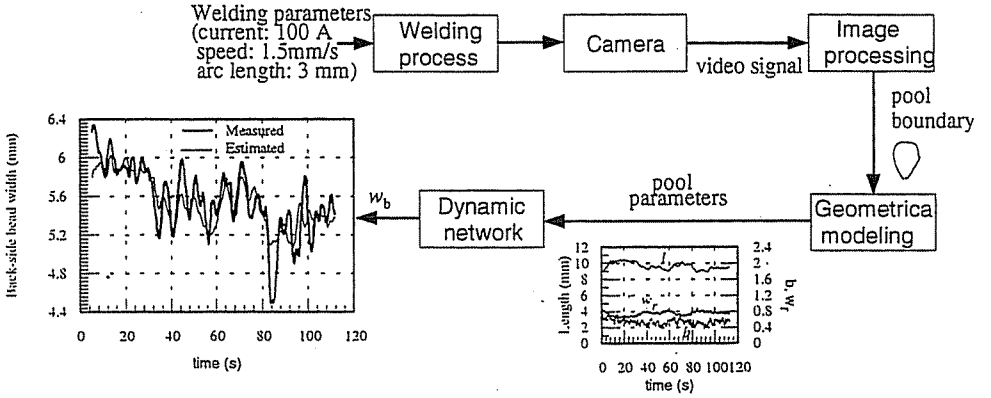

Fig. 15 On-line estimation of weld penetration

linear correlation with the back-side bead width. The gain is about 2 mm, rather than 5 mm in the linear model. The correlation between the pool length and weld penetration is not perfectly linear. The gain increases when the pool length increases. The maximum change of the gain is about 60 percent. The gain in the linear model (0.9) is basically an average estimate of the gain. This gain changes from 1.1 to 1.7 in the nonlinear model when $w_r = 0.6$ and $b = 0.4$. (It could change if w_r and b are different.) The most dramatic difference between the linear and non-linear models is caused by the length ratio. When the ratio increases from a small value (0.4), the weld penetration decreases very fast. (The gain can reach −7.0 mm.) When the ratio reaches about 0.8, the gain changes its sign. The weld penetration starts to increase with the length ratio. Thus, the correlation between the length ratio and the weld penetration is fundamentally non-linear. The gain $\alpha_3 = -1.69$ mm in the linear model is only a rough approximation of the correlation between the length ratio and weld penetration.

6.2 Improvement and Complexity. Although the improvement generated by the non-linear dynamic model is significant (Fig. 8 and Fig. 14), the accuracy associated with the

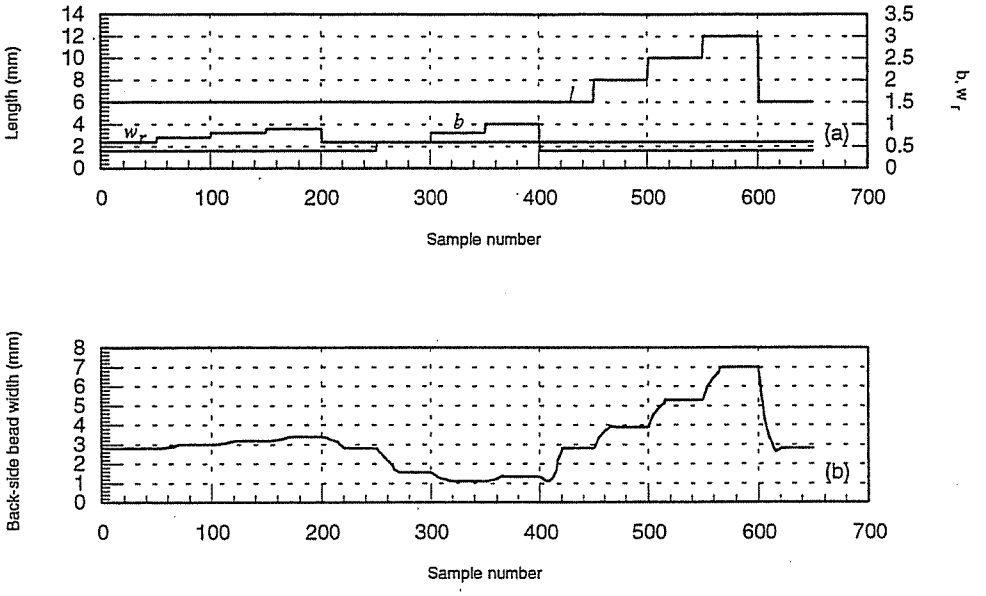

Fig. 16 Step responses of the dynamic neural network model

linear model could also be acceptable (Fig. 8) for most applications. Thus, for the simplification, the linear model could be used. However, the target of the developed estimation system is for the precise control of weld penetration. Thus, the authors prefer the non-linear dynamic model.

6.3 Variation in Dynamic Correlation. The responses of the back-side bead width to the step changes in the characteristic parameters have also been calculated using the neural networks trained using the experimental data from each individual experiment. It is seen that variations in the calculated back-side bead width exist among different models. This implies that the correlation between the weld pool parameters and back-side bead width is influenced by the experimental conditions and welding parameters which are different in each experiment. In our experiments, the travel speed has been changed from 1.5 mm/s to 3 mm/s. The current varies from 90 A to 130 A. The arc length covers the range from 1.5 mm to 6 mm. The variations in the step responses reflect the influence of the welding parameters and conditions on the correlation between weld pool and weld penetration. However, the observed variations in the step responses are not significant. Thus, the influence of the welding parameters and conditions on the correlation is slight.

6.4 Shift and Estimation. In the data preparation for the dynamic modeling, the optimal shifts j_0^*'s selected from different experiments have been used for the data in different experiments, although the used δ and n are the same for the data from different experiments. In practical welding, the exact value of the optimal j_0^* may not be available. An estimate of j_0^* can be used to implement the network calculation. Denote the estimate of j_0^* as $\hat{j}_0^*$. The difference between $\hat{j}_0^*$ and j_0^* will produce a phase shift in the resultant estimate. However, during weld penetration control, the desired status of the weld penetration is usually constant. In this case, the phase shift will produce no influence either on the weld quality or on the control actions of the welding process. In the case that the desired status varies, the resultant shift could influence the welds in the transient intervals. However, if j_0^* can be estimated, the resultant shift could be reduced to a minimum. The resultant influence on the welds could also be kept to a minimum.

7 Conclusions

The experiments have been performed on 3 mm stainless steel 304 plates using GTA welding. Pure argon is used as the shielding gas. The welding current varied from 90 A to 130 A. The travel speed varied in the range from 1.5 mm/s to 3 mm/s, and the arc length changed from 2 mm to 6 mm. Because of the changes in the welding parameters, weld pools with different geometrical appearances have been made. The resultant full penetration status, specified by the back-side bead width varied from 1 mm to 7 mm. Based on the above data, the following are found:

(1) The proposed normalized model can characterize the weld pool both in describing the geometrical appearance and in determining the weld penetration.

(2) The full penetration can be determined with sufficient accuracy by the proposed three characteristic parameters of the weld pool.

(3) The correlation between the weld pool and weld penetration is basically non-linear and dynamic. Specifically, the weld penetration increases when the pool length or relative width increases. The increase in the length ratio tends to decrease the weld penetration in most cases. The pool length plays the most significant part in determining the weld penetration.

(4) The status of the full penetration can be on-line estimated using the developed image processing algorithm and dynamic neural-network.

It can be noticed that this study has been done for the full penetration mode. For partial penetration, the depth of penetration may also be correlated to the geometry of the weld pool. However, a neural network modeling which requires abundant data may not be easy because of the difficulty in measuring the depth of penetration.

Acknowledgment

This work is supported by the National Science Foundation (DMI-9634735) and Allison Engine Company, Indianapolis, IN.

References

1 Xiao, Y. H., and Ouden, G. den, 1990, "A Study of GTA Weld Pool Oscillation," *Welding Journal,* Vol. 69, No. 8, pp. 298s–293s.

2 Xiao, Y. H., and Ouden, G. den, 1993, "Weld Pool Oscillation during GTA Welding of Mild Steel," *Welding Journal,* Vol. 72, No. 8, pp. 428s–434s.

3 Hoffman, T., 1991, "Real-time Imaging for Process Control," *Advanced Material & Processes,* Vol. 140, No. 3, pp. 37–43.

4 Kovacevic, R., Zhang, Y. M., and Ruan, S., 1995, "Sensing and Control of Weld Pool Geometry for Automated GTA Welding," ASME JOURNAL OF ENGINEERING FOR INDUSTRY, Vol. 117, No. 2, pp. 210–222.

5 Kotecki, D. J., Cheever, D. L., and Howden, D. G., 1972, "Mechanism of Ripple Formation During Weld Solidification," *Welding Journal,* Vol. 51, No. 8, pp. 386s–391s.

6 Renwick, R. J., and Richardson, R. W., 1983, "Experimental Investigation of GTA Weld Pool Oscillations," *Welding Journal,* Vol. 62, No. 2, pp. 29s–35s.

7 Zacksenhouse, M., and Hardt, D. E., 1984, "Weld Pool Impedance Identification for Size Measurement and Control," ASME *Journal of Dynamic Systems, Measurement, and Control,* Vol. 105, No. 3, pp. 179–184.

8 Hardt, D. E., and Katz, J. M., 1984, "Ultrasonic Measurement of Weld Penetration," *Welding Journal,* Vol. 63, No. 9, pp. 273s–281s.

9 Carlson, N. M., and Johnson, J. A., 1988, "Ultrasonic Sensing of Weld Pool Penetration," *Welding Journal,* Vol. 67, No. 11, pp. 239s–246s.

10 Carlson, N. M., et al., 1992, "Ultrasonic NDT Methods for Weld Sensing," *Material Evaluation,* Vol. 50, No. 11, pp. 1338–1343.

11 Yang, J., et al., 1994, "Ultrasonic Weld Penetration Depth Sensing With a Laser Phased Array," *Proceedings of 1994 ASME International Mechanical Engineering Congress,* PED-Vol. 68-1, *Manufacturing Science and Engineering,* pp. 245–254, Nov. 6–11, Chicago, IL.

12 Nagarajan, S., Chen, W. H., and Chin, B. A., 1989, "Infrared Sensing for Adaptive Arc Welding Control," *Welding Journal,* Vol. 68, No. 11, pp. 462s–466s.

13 Nagarajan, S., Banerjee, P., and Chin, B. A., 1990, "Weld Pool Size and Position Control Using IR Sensors," *Proceedings of NSF Design and Manufacturing Systems Conference,* Arizona State University, January 8–12.

14 Chen, W., and Chin, B. A., 1990, "Monitoring Joint Penetration Using Infrared Sensing Techniques," *Welding Journal,* Vol. 69, No. 4, pp. 181s–185s.

15 Song, J.-B., and Hardt, D. E., 1993, "Closed-loop Control of Weld Pool Depth Using a Thermally Based Depth Estimator," *Welding Journal,* Vol. 72, No. 10, pp. 471s–478s.

16 Song, J.-B., and Hardt, D. E., 1994, "Dynamic Modeling and Adaptive Control of the Gas Metal Arc Welding Process," ASME *Journal of Dynamic Systems, Measurement, and Control,* Vol. 116, No. 3, pp. 405–413.

17 Beardsley, H., Zhang, Y. M., and Kovacevic, R., 1994, "Infrared Sensing of Welding Parameters for Weld Penetration Control," *International Journal of Machine Tool and Manufacturing,* Vol. 34, No. 8, pp. 1079–1090.

18 Lin, M. L., and Eagar, T. W., 1984, "Influence of Surface Depression and Convection on Arc Weld Pool Geometry," *Transport Phenomena in Materials Processing,* ASME, New York, N.Y. 63–69.

19 Rokhlin, S. I., and Guu, A. C., 1993, "A Study of Arc Force, Pool Depression, and Weld Penetration During Gas Tungsten Arc Welding," *Welding Journal,* Vol. 72, No. 8, pp. 381s–390s.

20 Zhang, Y. M., Cao, Z. N., and Kovacevic, R., 1996, "Numerical Analysis of Fully Penetrated Welds in GTA Welding," *Proc. Instn. Mech. Engrs.,* Part C, *Journal of Mechanical Engineering Science,* Vol. 210, No. 2, pp. 187–195.

21 Zhang, Y. M., et al., 1993, "Determining Joint Penetration in GTAW With Vision Sensing of Weld Face Geometry," *Welding Journal,* Vol. 72, No. 10, pp. 463s–469s.

22 Zhang, Y. M., Kovacevic, R., and Wu, L., 1996, "Dynamic Modeling and Identification of Gas Tungsten Arc Welding Process for Weld Penetration Control," ASME JOURNAL OF ENGINEERING FOR INDUSTRY, Vol. 118, No. 1, pp. 123–136.

23 Zhang, Y. M., Kovacevic, R., and Li, L., 1996, "Adaptive Control of Full Penetration GTA Welding," *IEEE Transactions on Control Systems Technology,* Vol. 4, No. 4, pp. 394–403.

24 Richardson, R. W., et al., 1984, "Coaxial Arc Weld Pool Viewing for Process Monitoring and Control," *Welding Journal,* Vol. 63, No. 3, pp. 43–50.

25 Boyer, K., and Penix, W. A., 1992, "An Image Analysis System for Coaxially Viewed Weld Scenes," *Machine Vision and Applications,* Vol. 5, pp. 277–293.

26 Dawson-Howe, K. M., and Vernon, D., 1994, "Simple Pinhole Camera Calibration," *International Journal of Imaging Systems and Technology,* Vol. 5, pp. 1–6.

27 Pandit, S. M., and Wu, S. M., *Time Series and System Analysis With Applications,* Chp 2, John Wiley and Sons, New York, 1983.

28 Zhang, Y. M., and Kovacevic, R., 1996, "Real-time Sensing of Sag Geometry During GTA Welding," ASME JOURNAL OF MANUFACTURING SCIENCE AND ENGINEERING (*formerly* JOURNAL OF ENGINEERING FOR INDUSTRY), Vol. 119, No. 2, pp. 151–160.

29 Hunt, K. J., et al, 1992, "Neural Networks for Control Systems: A Survey," *Automatica,* Vol. 28, No. 6, pp. 1083–1112.

30 Using NeuralWorks: Professional II/Plus and NeuralWorks Explorer, NeuralWare Inc., Pittsburgh, PA, 1993.